

Article

# CORRELATION BETWEEN MICROSTRUCTURE AND CHEMICAL COMPOSITION OF ZINC OXIDE GAS SENSOR LAYERS AND THEIR GAS-SENSITIVE PROPERTIES IN CHLORINE ATMOSPHERE

Marta Fiedot-Toboła<sup>1,2)\*</sup>, Patrycja Suchorska-Woźniak<sup>1)</sup>, Kamila Startek<sup>2)</sup>,  
Olga Rac-Rumijowska<sup>1)</sup>, Rafał Szukiewicz<sup>3,2)</sup>, Monika Kwoka<sup>4)</sup>, Helena Teterycz<sup>1)</sup>

<sup>1</sup> Faculty of Electronics Microsystems and Photonics, Wrocław University of Science and Technology, Janiszewskiego 11/17, 50-372 Wrocław, Poland

<sup>2</sup> Łukasiewicz Research Network – PORT Polish Center for Technology Development, Stabłowicka 147, 54-066 Wrocław, Poland

<sup>3</sup> University of Wrocław, Institute Experimental Physics, Maxa Born'a 9, 50-204 Wrocław, Poland

<sup>4</sup> Institute of Electronics, Silesian University of Technology, Gliwice 44-100, Poland

\* Correspondence: marta.fiedot-tobola@port.org.pl, +48 71 734 71 54

**Abstract:** In the article we present the results concerning the impact of structural and chemical properties of zinc oxide in various morphological forms, on its gas-sensitive properties tested in an atmosphere containing a very aggressive gas such as chlorine. Two types of ZnO sensor layers obtained by two different technological methods were used. Their morphology, crystal structure, specific surface area, porosity, surface chemistry and structural defects were characterized, and then compared with gas-sensitive properties in a chlorine-containing atmosphere. To achieve this goal scanning electron microscopy (SEM), X-ray diffraction (XRD), X-ray photoelectron spectroscopy (XPS) and photoluminescence spectroscopy (PL) methods were used. The sensing properties of obtained active layers were tested by temperature stimulated conductance method (TSC). We have noticed that their response in chlorine atmosphere is not determined by the size of the specific surface or porosity. The obtained results showed that the structural defects of ZnO crystals play the most important role in chlorine detection. We demonstrated that the Cl<sub>2</sub> adsorption is a concurrent process to oxygen adsorption. Both of them occur on the same active species (oxygen vacancies). Their concentration is higher on the side planes of the zinc oxide crystal than the others. Thanks to the conducted studies authors demonstrated that to develop a new gas sensor devices not only changing of active layer chemical composition but also controlling its crystal structure and morphology could be used.

**Keywords:** resistive gas sensors, chlorine sensitivity, zinc oxide, microstructure, chemistry

## 1. Introduction

Resistive gas sensors due to their simple construction, low cost and large range of detectable gases as carbon monoxide [1], nitrogen oxides [2] or methane [3] are widely used in commercial gas detection systems. Gas-sensitive materials used in such sensor are made of metal oxides with semiconductor properties. The electrical parameters of these oxides, such as work function or conductance, depends on the composition of the atmosphere being tested. Despite a huge number of scientific studies conducted in this field, resistive gas sensors still exhibit an unsatisfactory selectivity [4–6]. Therefore, researches directed at searching for new materials in order to eliminate this defect are still being carried out [7–9]. Among other things, gas-sensitive materials of various

morphological forms and dimensions, undoped or catalytically doped with active nanoparticles are synthesized and tested [10–13].

In addition to research focusing on material engineering, studies on the mechanism of interaction of various gases with gas-sensitive material are very important. It is well known that the physicochemical processes that determine the sensor response occur at the gas-oxide semiconductor interface. For this reason, it is assumed that the basic parameters of the sensors, such as sensitivity, selectivity, response and recovery time, and stability are primarily determined by the specific surface area and porosity. These parameters are correlated and, according to literature reports, the most important one is the specific surface of the sensor material. It is widely believed that with the increase of the specific surface area of a material, the concentration of active centers increases, and therefore a greater number of atoms (or molecules) can participate in the physicochemical processes occurring at the gas-semiconductor interface. Among other things, that is why a lot of research concerns nanomaterials because they have the highest possible specific surface value [14–17]. For this reason, sensors made of nanomaterials should have better sensitivity, selectivity, stability and shorter response and recovery time [18].

In the field of nanotechnology, a lot of research relates to one-dimensional (1D) or quasi-one-dimensional (q-1D) zinc oxide structures have been performed [19–21]. The ZnO having the n-type semiconductor properties is characterized by: a large band gap, high exciton binding energy, high absorption of ultraviolet (UV) electromagnetic radiation, very good photocatalytic properties, and high electromechanical coupling factor. An extremely important advantage of ZnO is its ability to crystallize in various morphological forms such as rods, tubes, plates, core-shell structures, etc. [22–27]. Currently, various of them are used in the construction of different types of electrical components such as piezoelectric sensors, ultraviolet radiation sensors, biosensors, and resistance gas sensors. 1D and/or q-1D structures are characterized by a very large ratio of surface to volume of material and several methods are used to produce ZnO in this form [28]. Chemical bath deposition (CBD) is one of the most popular method used to achieve this goal, because it is carried out at a low temperature, it does not require the use of complicated equipment, and the change in process parameters allows modification of the microstructure of the obtained zinc oxide forms. According to literature reports, it is also possible to produce q-1D ZnO structures directly on ceramic substrates, and the gas-sensitive layers thus obtained are characterized by better parameters compared to their volume equivalents [29,30].

In this article, we present the results of the impact of ZnO structural and chemical properties on its gas-sensitive properties in the atmosphere containing an very aggressive chlorine gas. Two types of ZnO layers obtained with the different methods were tested. Their morphology, crystal structure, specific surface, porosity were characterized were determined, then they were correlated with gas-sensitive properties in a chlorine-containing atmosphere. The preliminary results in this field the authors have presented in recent paper [31]. Due to the fact that the mechanism of interaction of chlorine with gas-sensitive oxides is little known, as illustrated by a small number of publications on this subject [32,33], the article also presents a critical analysis of the obtained results. A lot of attention was mainly devoted to determining the correlation between the structural and gas-sensitive properties of zinc oxide and a chlorine detection mechanism was proposed.

## 2. Materials and Methods

Our gas-sensitive layers based on ZnO were made by thick-film technology and CBD method on a substrate with electrodes and a heater. The thickness of the alundum substrate (96% Al<sub>2</sub>O<sub>3</sub>) with dimensions of 25.40 × 2.45 mm<sup>2</sup> was 250 μm. On one side of the substrate there was a platinum heater in the form of a meander and gold contacts (ESL 8846-G, ESL Europe, Reading, England). On the other side the gold Au electrodes and dielectric (ESL 4913-G, ESL Europe, Reading, England) were printed as shown in the Figure 1.

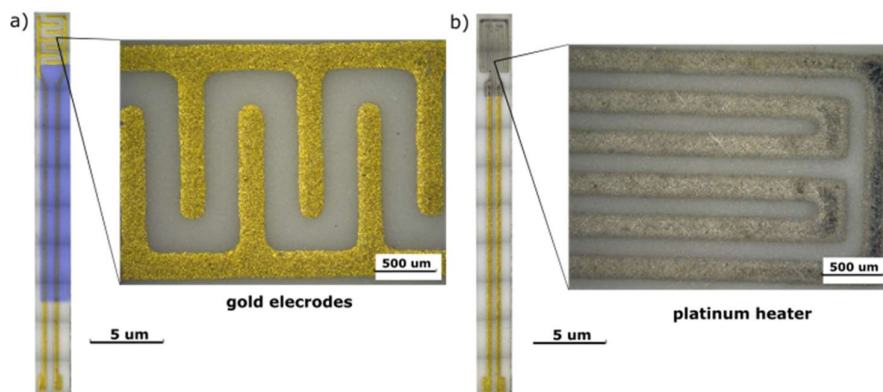


**Figure 1.** Images of the gas sensor surface from the side of: a) gold electrodes, b) heater.

The q-1D ZnO structures were deposited only on the side of the substrate on which the electrodes were located. The process was carried out with the chemical bath deposition method in an equimolar solution of aqueous zinc nitrate ( $\text{Zn}(\text{NO}_3)_2$ ) and hexamethylenetetramine (HMT). In the first stage of process, a zinc nitrate solution and a HMT solutions were prepared, each at a concentration of 1 M. Then, both solutions were mixed together in a 1:1 ratio and diluted, thus the final concentration of individual compounds was 100 mM. The structure growth process was carried out at a temperature of 90°C for 9 hours, at atmospheric pressure. After the process was completed, the sensor structures were rinsed in deionized water in an ultrasonic cleaner and then dried in an ambient atmosphere [34].

The ZnO powder was prepared by the precipitation of zinc chloride with sodium hydroxide. The reaction was carried out at 90°C. The resulting precipitate was washed in deionized water, then dried at room temperature. In order to make the sensor layer, using the screen printing technique, a paste made of zinc oxide powder and organic carrier (ESL-403, ESL Europe, Reading, England) was prepared. The paste was printed twice with a DEK 1202 screen printer, by drying the layers after each printing, first at room temperature and then at 125°C for 10 minutes. The structure of sensor was fired in a tunnel furnace according to a standard profile. The maximum temperature was 850°C for 10 min. The thickness of ZnO layer was about 40  $\mu\text{m}$ .

The surface morphology of our ZnO sensor layers was examined using SEM (Zeiss Evo LS 15).

The crystal structure of the formed ZnO layers was examined by XRD (Philips Materials Research Diffractometer, MRD with  $\text{CuK}\alpha$  radiation). On the basis of characteristic peaks, the average size of crystallites and microstrains in the ZnO structures were determined with the Williamson-Hall (W-H) method [35].

The porosity analysis of obtained sensor layers was performed on the base of Brunauer-Emmett-Teller (BET) multilayer adsorption isotherms. The ZnO structures in a powder form were prepared for the tests with CBD method. The synthesis of these structures was carried out under the same conditions in which they grew directly on alundum substrates. Zinc oxide powders were degassed in a Smart VacPrep preparation station at 200°C for 6 hours. After this time, they were placed in a Micromeritics 3Flex analyser and adsorption and desorption isotherms at liquid nitrogen temperature were determined. Nitrogen with a purity of 6.0 (as the adsorbate) and helium with a purity of 6.0 (for measuring empty space) were used in the measurements. In addition to the specific BET surface area, pore volume and average pore size were also determined using the Barrett-Joyner-Halend (BJH) method.

The surface chemical composition of our ZnO layers was determined by using XPS. The monochromatized X-ray source based on Al anode lamp (Al  $\text{K}\alpha$  emission line) was used. High-resolution photoelectron energy spectra were recorded using a SCIENTA EW3000 hemispherical analyser. The pressure in chamber during measurements was less than  $1 \times 10^{-9}$  mbar. To prevent sample charging, a low energy electron flood source was used. The samples were placed on a dedicated sample holder and introduced into the loading chamber, when the pressure reached

$2 \times 10^{-8}$  mbar. After approx. 1 h, the samples were placed in the XPS chamber and XPS measurement was performed. The CasaXPS software was used for results deconvolution. The concentration of atoms in individual samples was determined on the basis of XPS spectra analysis, taking into account the presence of individual elements O1s, C1s and Zn3s.

PL measurements were performed to determine the impact of ZnO preparation method on the type and density of defects inside the crystal structure. The measuring system was equipped with a He Cd 325 nm continuous laser, detector (CCD camera) and an optical system. The measurement was made at room temperature in atmospheric air. The signal acquisition time was 1000 min. The final results are based on the five subsequent scans.

The gas-sensitive properties of sensors with various form of ZnO layers were analysed in ambient air and in an atmosphere containing 2 ppm of chlorine gas. In both atmospheres a relative humidity was 40%. As was mentioned above the change in ZnO layer resistance under the influence of chlorine was determined by TSC method. During these measurements the current flowing through the sensor material was recorded whereas the temperature was cyclically changed in the range 150-750°C. The electrodes were polarized with a direct voltage of 2 V for thick layer and 50 mV for microrods. The temperature was changed at a rate of 2°C/s. The measuring system consisted of a Keithley 2400 (Keithley Instruments Inc., Cleveland, OH, USA) current and voltage source, HP E3632 power supply (Agilent Technologies Inc., Santa Clara, CA, USA), a Keithley 2400 current and voltage source, and a Solartron SI 1287 galvanostat potentiostat.

### 3. Results

#### 3.1. Structural Characterisation

The morphology of ZnO layers obtained by screen printing and CBD was observed using SEM method. The microstructure of the obtained oxide layers varied visibly. A thick layer of ZnO, made by screen printing, was porous and made of grains of irregular shapes and various dimensions (Figure 2a). The layer formed as a result of a hydrothermal process was made of pointed q-1D zinc oxide microrods. The side walls of these structures were well formed (Figure 2b).

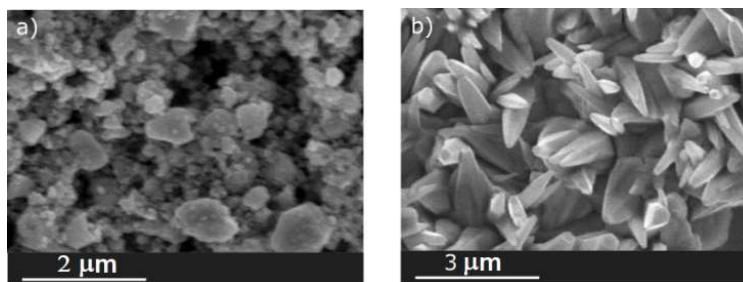


**Figure 2.** SEM images of ZnO layers formed with the method: a) screen printing; b) CBD.

Based on the XRD diffraction pattern analysis, it was found that both types of layers are made of ZnO with a wurtzite type structure (Zincite, JCPDS 5-0664). Since the layers synthesized by the hydrothermal method were formed directly on the electrode substrate, the X-ray diffraction patterns also show peaks characteristic of gold (electrode) and alundum ceramics (substrate). These peaks do not appear on the zinc oxide diffractograms used in screen printing, because ZnO powder was used to form the paste for XRD testing (Figure 3). Before testing, the powder was subjected to the same heat treatment as the printed layers.

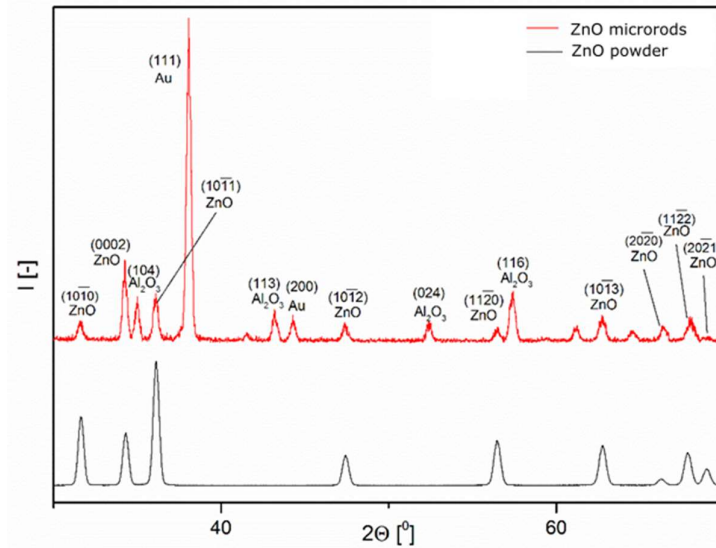


**Figure 3.** X-ray diffraction patterns of ZnO layers synthesized with two different methods.

The microstrains ( $\varepsilon$ ) and the size of crystallites ( $D$ ) were determined with the Williamson-Hall method (1) [35]. It was found that the size of ZnO crystallites forming a thick layer is 22 nm and it is clearly smaller than that of the structures obtained by the hydrothermal method (40 nm). Also, the microstrains value is definitely smaller and amounts to:  $5.8 \times 10^{-4}$  for the thick layer and  $15.8 \times 10^{-4}$  for q1-D structures [31].

$$\beta_{hkl} \cos(\theta) = \frac{k\lambda}{D} + 4\varepsilon \sin(\theta) \quad (1)$$

where:  $\beta$  – peak half width (FWHM),  $\theta$  – Bragg angle,  $k$  – Scherrer constant (0.9),  $\lambda$  – wavelength of Cu-K $\alpha$  radiation,  $D$  – crystallite size,  $\varepsilon$  – lattice strain.

The specific surface area and porosity of the sensor materials were determined with the method of physical nitrogen adsorption based on the adsorption isotherm analysis. Our studies have shown that both sensing materials are mesoporous. The specific surface, pore volume and average pore diameter of the powder used in screen printing is several times bigger than in the structures created in the hydrothermal process (Figure 4).

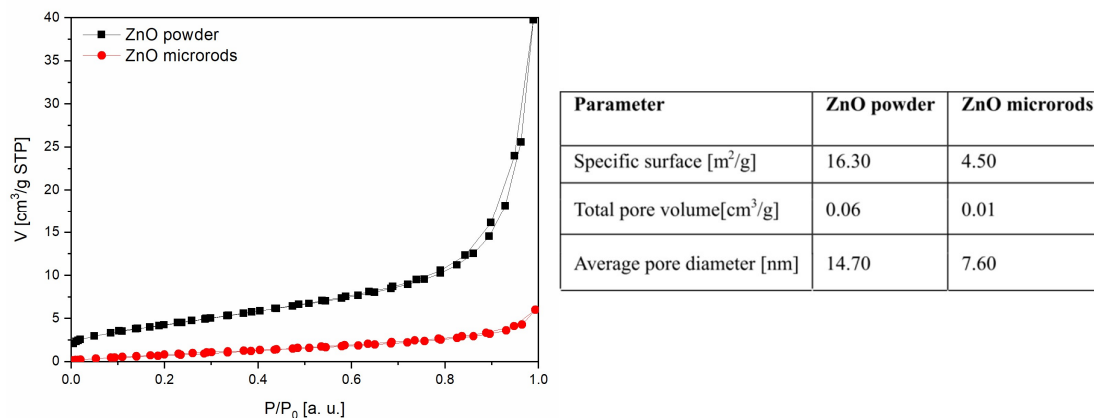


**Figure 4.** Isotherms of N<sub>2</sub> adsorption/desorption and BET analysis results of the samples.

As was mentioned earlier, the surface chemical composition of both ZnO layers was determined by XPS method. The spectra of these materials show peaks confirming the presence of

such elements as: zinc ( $Zn2p_{1/2}$ ,  $Zn2p_{3/2}$ ,  $Zn3s$ ,  $Zn3p$ ,  $Zn3d$ ), oxygen ( $O1s$ ) and carbon ( $C1s$ ). The presence of carbon in the samples indicates the adsorption of organic substances on the surface of our samples or carbon dioxide from the atmosphere (Figure 5). On the base of our XPS results it was found that on the surface of microrods the relative concentration of carbon  $C1s$  (24.27%) is higher than on the surface of a thick layer (8.77%). It results from the presence of some organic compounds remaining after hydrothermal synthesis. In addition, it was found that for both samples the ratio of  $Zn/O$  is about 0.97. Therefore, there is a slightly higher amount of oxygen on the surface compared to zinc, which confirms the phenomenon of oxygen sorption on the surface of the oxide semiconductor.

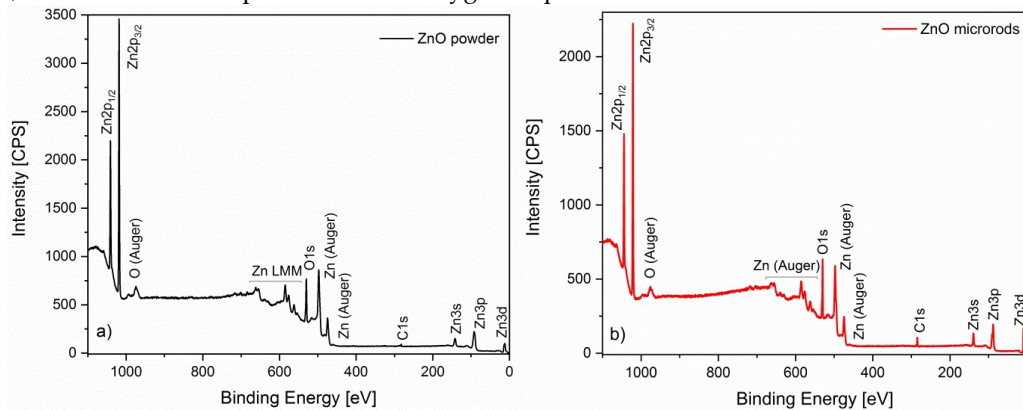


**Figure 5.** Zinc oxide XPS spectra in the form of; a) powder; b) microrods.

The oxygen forms (surface bondings) on the ZnO surface of our both samples were determined on the base of deconvolution of the XPS  $O1s$  spectral lines and the relative intensity of the recognized components. For the ZnO microrods the XPS  $O1s$  spectral line consists of three components (Figure 6a). According to literature reports, these peaks are associated with:  $O^2$  species in the lattice ( $O_L$ , 530 eV), oxygen vacancies or defects ( $O_V$ , 531.4 eV) and oxygen adsorbed on the surface of ZnO ( $O_A$ , 532.4 eV), as proposed in the recent literature papers [36–38]. In turn, for the XPS  $O1s$  spectral line of ZnO layer made by screen printing the component corresponding to oxygen vacancies at 531.4 eV was not observed. Furthermore, the two other components of XPS  $O1s$  spectral lines have different FWHM (Full width at half maximum) with respect to those observed for ZnO microrods (Figure 6b).

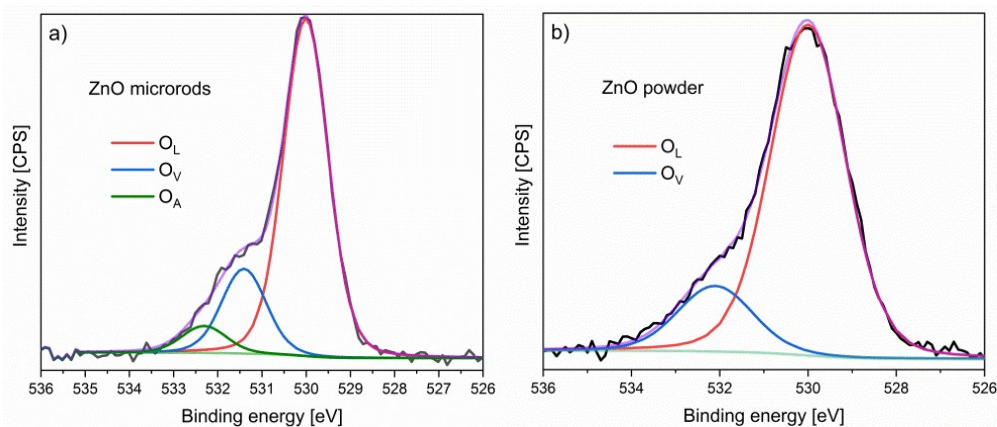


**Figure 6.** XPS  $O1s$  spectral lines after deconvolution of ZnO: a) powder, b) microrods.

As was mentioned above, the photoluminescence (PL) tests were performed to determine the type and concentration of defects occurring in the ZnO crystal structure. Studies have shown the existence of significant differences in the emission bands of the tested oxides synthesized with various methods and, as a consequence, differing in microstructure. Both in the thick layer spectrum

and in the microrod layer there is an energy maximum around 380 nm associated with the transition of electrons between valence and conductivity band. Further peaks in the PL spectrum are associated with the presence of certain structural defects in the oxide. In both forms of ZnO, oxygen vacancies and oxygen atoms were found in interstitial positions [39,40]. In case of microrods, oxygen vacancies are clearly the dominant defect, whereas in case of ZnO powder, interstitial oxygen is the dominant defect (Figure 7).

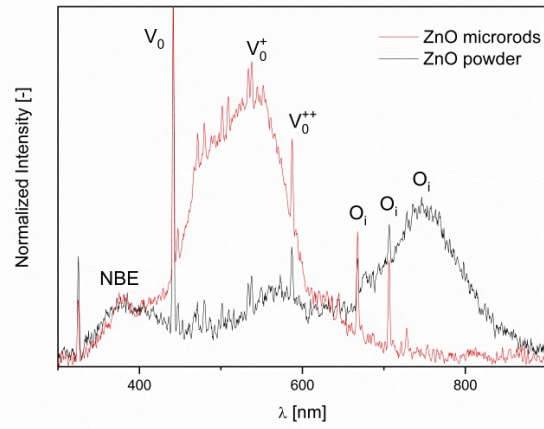


Figure 7. PL spectra of ZnO samples.

### 3.2. Analysis of gas-sensitive properties

Gas-sensitive properties of the obtained ZnO layers in the chlorine atmosphere were determined by TSC method. Based on these tests the sensitivity of the sensors was calculated. Sensor sensitivity ( $S$ ) is the measurement of the sensor response relative to the determined gas and it is defined as a derivative of the processing function after the measured non-electrical quantity (2). Determining the analytical form of this function is extremely difficult. For this reason, the sensitivity of the sensor is commonly defined as the ratio of the sensor signal (conductance) value in the analysed atmosphere to the value of the signal in the reference atmosphere (3). Because chlorine is an oxidizing gas and causes a decrease in the conductivity of the gas-sensitive material, sensitivity was defined as the ratio of the layer conductance value in the reference atmosphere to the conductivity in the atmosphere containing  $\text{Cl}_2$  (4) so that the value of sensitivity is greater than 1 [8].

$$S = \frac{df}{dx} \quad (2)$$

$$S = \frac{G_{\text{gas}}}{G_0} \quad (3)$$

$$S = \frac{G_0}{G_{\text{Cl}_2}} \quad (4)$$

where:  $G_0$  - layer conductance in the reference atmosphere,  $G_{\text{gas}}$  - layer conductance in the atmosphere containing the detecting gas,  $G_{\text{Cl}_2}$  - the conductance of the layer in the atmosphere containing chlorine.

The analysis of obtained results showed that the conductivity of both ZnO layers of various microstructure and other physiochemical properties, decreases in the presence of chlorine. This result confirms the oxidative nature of chlorine gas. However, the conductance in the air of the layer made of microrods was definitely higher with respect to the thick layer (Figure 8a). These differences are more clearly visible on the characteristics of  $S$  value vs temperature. The ZnO layer made by screen printing is much less sensitive than the layer made of microrods. In addition, the variation of sensitivity as a function of temperature also differ significantly. They indicate the occurrence of differences in the kinetics of interaction of chlorine with the surface of ZnO layers, which differs in microstructure and the type and concentration of defects (Figure 8b).

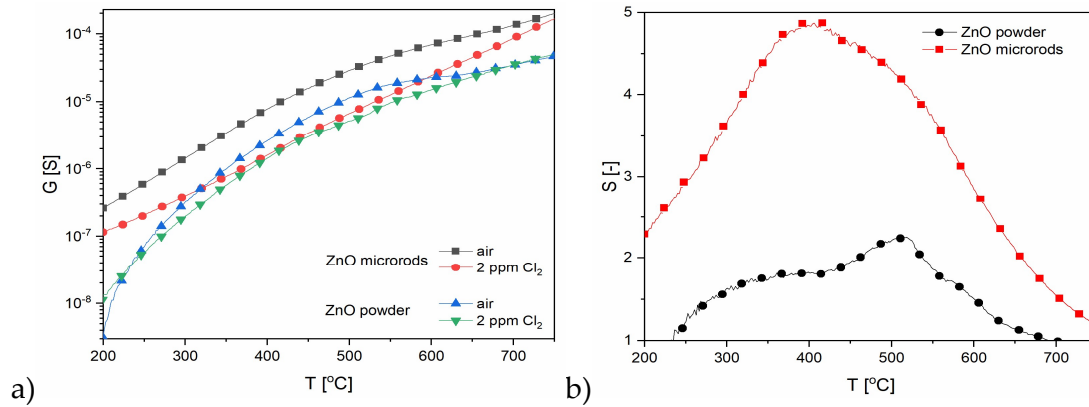


**Figure 8.** Temperature changes of: a) conductance; b) sensitivity to  $Cl_2$  of the sensors.

#### 4. Discussion

In order to explain the differences in behaviour of our both ZnO layers, an attempt was made to determine the relationship between the microstructure and ZnO gas-sensitive properties and the mechanism of gas sensing phenomena occurring on the surface of zinc oxide in the presence of chlorine.

It is well known that some gases interact with the surface of various metal oxides, triggering a change in their conductance (resistance). Depending on the nature of chosen gas and the type of metal oxide conductivity, the resistivity of the gas-sensitive material decreases or increases.

In case of n-type semiconductors, e.g. ZnO, their conductivity decreases in the presence of oxidizing gas and increases in the presence of reducing gases. In the reference atmosphere, mainly oxygen is adsorbed on the surface of metal oxide. Oxygen is characterized by high electronegativity and its concentration in the ambient atmosphere is relatively high (about 200,000 ppm). For this reason, it is easily chemisorbed on the surface of metal oxides, in which oxygen vacancies are the dominant defects. The phenomenon occurs at every temperature  $T$ . At higher  $T$  values, oxygen undergoes chemisorption and becomes an ion  $O_2^-$ ,  $O^-$  or  $O^{2-}$  as a result of electron/electrons attachment from the semiconductor conductivity band. Göpel found that the maximum amount of oxygen  $\Theta_{max}$  (degree of surface coverage), which can undergo chemisorption is less than  $\leq 2,5 \times 10^{-4}$  [41]. Because in the chemisorption process of oxygen a charge exchange occurs on the surface of gas-sensitive material, the core-shell structure is created as a result of this process. The outer layer (shell) has a larger and the inside (core) has a smaller resistance (Figure 9). The oxygen-metal interaction is directly related to the width of layer (shell) depleted in electrons and the height of surface potential barrier formed at the grain boundary [14].

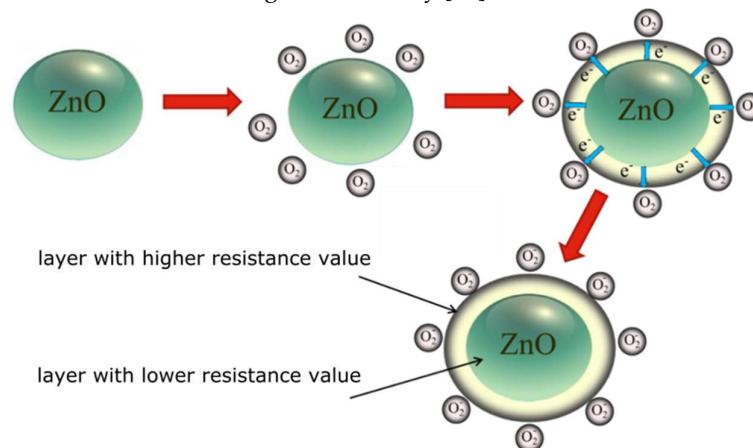


**Figure 9.** Diagram of the chemical sorption process of oxygen on the surface of an n-type oxide semiconductor.

When chlorine, which is also an oxidizing gas, appears in the atmosphere surrounding the sensor material, a number of competitive processes take place.

According to literature data, chlorine can form chlorine oxide (5), displace chemically adsorbed oxygen (6), substitute oxygen in nodal positions ( $O_0^x$ ) (7) and fill oxygen gaps ( $V''$ ) (8). It is believed that all these processes cause a decrease in conductance of the n-type semiconductor gas-sensitive material in the presence of chlorine [33,42].

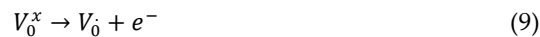


The analysis of thermodynamic data rules out the possibility of chlorine oxides formation (5) because Gibbs free energy of formation of these compounds is negative and depending on the degree of chlorine oxidation takes values in the range from -18.3 to -63.4 kcal/mol.[43] Moreover, chlorine oxides are not formed as a result of a direct reaction of chlorine with oxygen, chlorine oxides are highly reactive and easily undergo explosive decomposition.[43] As far as chlorine substitution oxygen reactions are concerned (6, 7), the possibility of their occurrence should also be ruled out, since the electronegativity of chlorine is lower than that of oxygen ( $3.0 < 3.5$ ) and the concentration of oxygen is several orders higher than the concentration of chlorine (200,000 ppm > 2 ppm). Therefore, in case of chlorine detection, only reactions related to competitive chemical adsorption of chlorine on surface oxygen vacancies should be taken into account (8).

In this study, the conditions for the characterization of both ZnO were identical, therefore explanations for the differences in their behaviour in the presence of chlorine gas were attributed to the differences in the structural and chemical properties of the gas-sensitive layer. It is widely believed that the bigger the specific surface of a gas-sensitive material, the greater its sensitivity will be as chemisorption of gases is a process that occurs on the surface of a semiconductor [19]. The analysis of obtained our results does not confirm this claim. However, the sensor layer made of microrods is characterized by a higher sensitivity in a chlorine-containing atmosphere, despite the fact that the specific surface area of the powder is more than three times and the pore diameter is almost twice bigger than in the case of microrods (Figure 4).

As it is well known, adsorption does not occur on the entire adsorbent surface, but on active centres. For this reason, not only the size of specific surface is important, but also the concentration of individual defects, which usually form active centres.

Han et al. has postulated that semiconductor crystal lattice defects are crucial during oxygen adsorption. As it has already been mentioned, during the interaction of this gas with the ZnO surface, an exchange of charge (electrons) occurs. Therefore, it is preferred that the oxide has as many donor and as few acceptor levels as possible. Oxygen vacancies are the defects causing an increase in the concentration of donor levels in zinc oxide (9, 10) and interstitial oxygen causes their decrease (11, 12) [44].



where:  $V_0^x$  – oxygen gap;  $V_0, V_0'$  – positive charge oxygen gap;  $O_i^0$  – oxygen atom in the interstitial position;  $O_i^-, O_i^{2-}$  – negative oxygen ion in the interstitial position.

Thus, the rate of chemisorption process is proportional to the concentration of donor defects (oxygen vacancies), partial pressure of chemisorbed molecules, and activation energy (13).

$$v_{ads\ chem} = [V_O^{\bullet}] \cdot \exp\left(\frac{E_a}{kT}\right) \cdot p_{gas} \quad (13)$$

where:  $v_{ads\ chem}$  - speed of the chemisorption process,  $E_a$  - activation energy,  $p_{gas}$  - gas partial pressure,  $k$  - Boltzmann constant,  $T$  - temperature.

Because the rate of chemisorption process, which is associated with the exchange of electric charge, determines the response of sensor material, the relationship (13) shows that if the sensor material contains more vacancies, its response will be greater.

Our XPS and PL studies have shown that ZnO microrods contain significantly more oxygen vacancies than ZnO powder (Figure 6, 7). For this reason, both the chemical adsorption of oxygen and chlorine should occur more intensively on the surface of microrods. In our studies we have observed a similar dependency and their relationship with ZnO morphology. It was found that the most oxygen vacancies are concentrated on the side planes of the zinc oxide crystal [45,46]. This phenomenon could also explain higher sensitivity value in the case of ZnO microrods than powder in our studies. This is also consistent with Göpel's claim [41] because an achieving of maximum oxygen coverage at the surface will impede, but not reduce, the chlorine chemisorption. This theorem explains the greater sensitivity of ZnO microrods but does not explain the differences in temperature sensitivity changes (Figure 8b).

As it has already been suggested, chlorine and oxygen adsorption are two competitive processes (8, 13), as evidenced by the shape of the characteristics of temperature sensitivity changes. For our both gas-sensitive layers, the  $S$  value gradually increases until it reaches its maximum and then decreases. The curves illustrating these changes can be simulated with two peaks illustrating two different processes determining the response of a layer in a chlorine-containing atmosphere (Figure 10). It was assumed that the first peak depends on the intensity of oxygen interaction with the semiconductor surface. The obtained results were correlated with various physicochemical processes occurring in the ZnO layers in the atmosphere containing oxygen, as described in the literature.

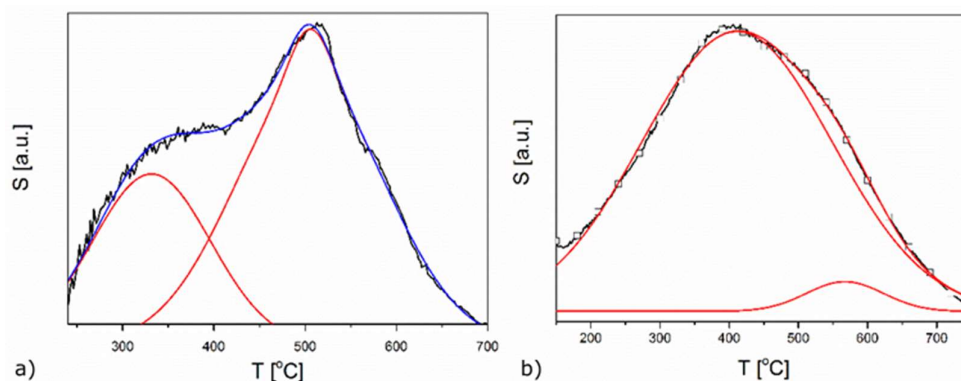


**Figure 10.** Sensitivity simulation to 2 ppm  $\text{Cl}_2$  as a function of temperature of: a) powder, b) microrods.

According to Göpel, the chemical adsorption of oxygen on the zinc oxide surface begins at 21°C and reaches its maximum value at 165°C. At 304°C, the gas is desorbed and the maximum occurs at 481°C. However, below this temperature ZnO a sublimation effect begins. If the material is heavily defective, the beginning of sublimation has already been found at 360°C [41].

Comparing the literature data with our obtained temperature changes in sensitivity, it should be stated that when using ZnO layers for the detection of chlorine very important is the interaction of chlorine with oxygen vacancies and ZnO sublimation process speed. In case of both zinc oxide layers, differing in microstructure, when the chemical adsorption rate of oxygen decreases and the desorption process of chemisorbed oxygen begins, the sensitivity increases. This is consistent with the statement that chlorine does not react with chemically adsorbed oxygen (6), nor is it able to



microrods. However, a ZnO layer made of microrods manifested a greater value of sensitivity in the presence of chlorine than a fine-crystal one, made by screen printing. The obtained results are in a contradiction to the generally accepted views on the direct correlation between sensitivity and the size of active surface. The thick ZnO layer characterized by almost four times bigger specific surface area than microrods exhibits twice as low sensitivity. This is probably related to the differences in microstructure and differences in the concentration of oxygen vacancies. The comparative analysis of literature data and our results showed that the main parameter determining the sensitivity of chlorine gas detection is the concentration of donor levels (oxygen vacancies) related to the ZnO microstructure. Both the concentration of oxygen vacancies and the microstructure of this ZnO layers depend on their synthesis method. The photoluminescence tests have clearly shown that in microrods donor defects, i.e. oxygen vacancies, are the dominant defects. In the granular structure of the thick ZnO layer, the dominant defects are interstitial oxygen. It has been shown that in a chlorine-containing atmosphere, this gas interacts with the free surface vacancies of ZnO. This reaction is a competitive process for the chemical sorption of oxygen at the surface oxygen vacancies. However, the concentration of surface vacancies in ZnO is not being constant because at a temperature higher than 350°C the sublimation of oxide begins, of rate depending on the ZnO microstructure. As a result of sublimation effect, the new surface vacancies are revealed that are not filled with oxygen, which can be occupied by chlorine. Based on the results of our performed studies it can be stated that the physicochemical processes occurring on the surface of gas-sensitive materials depend not only on such basic material parameters as the specific surface and porosity, but also on the degree and type of defects, the properties of chosen gas and the specific properties of gas-sensitive material such as temperature and the speed of sublimation. Both the degree and type of defects can be modified by using the various synthesis technique, as well as in the parameters of gas-sensitive material synthesis methods. As a consequence also sublimation rate will change can also be obtained.

**Author Contributions:** The manuscript was written through contributions of all authors. All authors have given approval to the final version of the manuscript. M. Fiedot-Toboła was planned and conducted experiments, analyzed the results and wrote the manuscript. P. Suchorska-Woźniak helped by measuring sensing properties and editing the article. K. Startek performed BET analysis. O. Rac-Rumijowska prepared ZnO powders. R. Szukiewicz and M. Kwoka did XPS analysis. H. Teterycz supervised whole work.

**Funding:** The research was founded through statutory funds from the Wrocław University of Science and Technology, Faculty of Microsystem Electronics and Photonics.

## References

1. Williams, D. E. Semiconducting oxides as gas-sensitive resistors. *Sensors Actuators B Chem.* **1999**, *57*, 1–16, doi:10.1016/S0925-4005(99)00133-1.
2. Urasinska-Wojcik, B.; Vincent, T.; ... M. C.-S. and A. B.; 2017, undefined Ultrasensitive WO<sub>3</sub> gas sensors for NO<sub>2</sub> detection in air and low oxygen environment. *Elsevier*.
3. Wei, H.; Kumar, P.; Science, D. Y.-E. J. of S. S.; 2020, undefined Printed Resistive Sensor Array Combined with a Flexible Substrate for Ethanol and Methane Detection. *iopscience.iop.org* **2020**, doi:10.1149/2162-8777/ab9fe6.
4. Lin, T.; Lv, X.; Hu, Z.; Xu, A.; Feng, C. Semiconductor metal oxides as chemoresistive sensors for detecting volatile organic compounds. *Sensors (Switzerland)* **2019**, *19*.
5. Halek, G.; Baikie, I. D.; Teterycz, H.; Halek, P.; Suchorska-Woźniak, P.; Wiśniewski, K. Work function analysis of gas sensitive WO<sub>3</sub> layers with Pt doping. *Sensors Actuators, B Chem.* **2013**, *187*, 379–385, doi:10.1016/j.snb.2012.12.062.
6. Nitsch, K.; Licznarski, B. W.; Teterycz, H.; Golonka, L. J.; Wiśniewski, K. AC equivalent circuits of thick film humidity sensors. *Vacuum* **1998**, *50*, 131–137, doi:10.1016/s0042-207x(98)00105-5.
7. Yamazoe, N. Toward innovations of gas sensor technology. In *Sensors and Actuators, B: Chemical*; 2005; Vol. 108, pp. 2–14.
8. Deng, Y.; Deng, Y. Sensing Mechanism and Evaluation Criteria of Semiconducting Metal Oxides Gas Sensors. In *Semiconducting Metal Oxides for Gas Sensing*; Springer Singapore, 2019; pp. 23–51.
9. Roy, P. K.; Haider, G.; Chou, T. C.; Chen, K. H.; Chen, L. C.; Chen, Y. F.; Liang, C. Te Ultrasensitive gas

- sensors based on vertical graphene nanowalls/SiC/Si Heterostructure. *ACS Sensors* **2019**, *4*, 406–412, doi:10.1021/acssensors.8b01312.
10. Suchorska-Woźniak, P.; Rac, O.; Klimkiewicz, R.; Fiedot, M.; Teterycz, H. Dehydrogenation properties of ZnO and the impact of gold nanoparticles on the process. *Appl. Catal. A Gen.* **2016**, *514*, 135–145, doi:10.1016/J.APCATA.2016.01.020.
  11. Franke, M. E.; Koplin, T. J.; Simon, U. Metal and metal oxide nanoparticles in chemiresistors: Does the nanoscale matter? *Small* **2006**, *2*, 36–50.
  12. Navazani, S.; Shokuhfar, A.; Hassanisadi, M.; Di Carlo, A.; Yaghoobi Nia, N.; Agresti, A. A PdPt decorated SnO<sub>2</sub>-rGO nanohybrid for high-performance resistive sensing of methane. *J. Taiwan Inst. Chem. Eng.* **2019**, *95*, 438–451, doi:10.1016/j.jtice.2018.08.019.
  13. Wang, C.; Cui, X.; Liu, J.; Zhou, X.; Cheng, X.; Sun, P.; Hu, X.; Li, X.; Zheng, J.; Lu, G. Design of Superior Ethanol Gas Sensor Based on Al-Doped NiO Nanorod-Flowers. *ACS Sensors* **2016**, *1*, 131–136, doi:10.1021/acssensors.5b00123.
  14. Barsan, N.; Weimar, U. Conduction Model of Metal Oxide Gas Sensors. *J. Electroceramics* **2001**, *7*, 143–167, doi:10.1023/A:1014405811371.
  15. Kolmakov, A.; Moskovits, M. CHEMICAL SENSING AND CATALYSIS BY ONE-DIMENSIONAL METAL-OXIDE NANOSTRUCTURES. *Annu. Rev. Mater. Res.* **2004**, *34*, 151–180, doi:10.1146/annurev.matsci.34.040203.112141.
  16. Suematsu, K.; Watanabe, K.; Tou, A.; Sun, Y.; Shimano, K. Ultrasensitive Toluene-Gas Sensor: Nanosized Gold Loaded on Zinc Oxide Nanoparticles. *Anal. Chem.* **2018**, *90*, 1959–1966, doi:10.1021/acs.analchem.7b04048.
  17. Hoang, T.; Doan, P.; Thanh, Q.; Ta, H.; Sreedhar, A.; Hang, N. T.; Yang, W.; Noh, J. Highly Deformable Fabric Gas Sensors Integrating Multidimensional Functional Nanostructures. **2020**, *5*, doi:10.1021/acssensors.0c01083.
  18. Kolmakov, A.; Moskovits, M. CHEMICAL SENSING AND CATALYSIS BY ONE-DIMENSIONAL METAL-OXIDE NANOSTRUCTURES. *Annu. Rev. Mater. Res.* **2004**, *34*, 151–180, doi:10.1146/annurev.matsci.34.040203.112141.
  19. Kuchibhatla, S. V. N. T.; Karakoti, A. S.; Bera, D.; Seal, S. One dimensional nanostructured materials. *Prog. Mater. Sci.* **2007**, *52*, 699–913, doi:10.1016/J.PMATSCI.2006.08.001.
  20. Masuda, Y.; Kato, K. Aqueous synthesis of ZnO rod arrays for molecular sensor. *Cryst. Growth Des.* **2009**, *9*, 3083–3088, doi:10.1021/cg800811j.
  21. Vallejos, S.; Pizúrová, N.; Gràcia, I.; Sotelo-Vazquez, C.; Čechal, J.; Blackman, C.; Parkin, I.; Cané, C. ZnO Rods with Exposed {100} Facets Grown via a Self-Catalyzed Vapor-Solid Mechanism and Their Photocatalytic and Gas Sensing Properties. *ACS Appl. Mater. Interfaces* **2016**, *8*, 33335–33342, doi:10.1021/acscami.6b12992.
  22. Zhou, X.; Wang, A.; Wang, Y.; Bian, L.; Yang, Z.; Bian, Y.; Gong, Y.; Wu, X.; Han, N.; Chen, Y. Crystal-Defect-Dependent Gas-Sensing Mechanism of the Single ZnO Nanowire Sensors. *ACS Sensors* **2018**, *3*, 2385–2393, doi:10.1021/acssensors.8b00792.
  23. Rocha, L. S. R.; Foschini, C. R.; Silva, C. C.; Longo, E.; Simões, A. Z. Novel ozone gas sensor based on ZnO nanostructures grown by the microwave-assisted hydrothermal route. *Ceram. Int.* **2016**, *42*, 4539–4545, doi:10.1016/J.CERAMINT.2015.11.145.
  24. Chen, L.; Cui, J.; Sheng, X.; Xie, T.; Xu, T.; Feng, X. High-Performance Photoelectronic Sensor Using Mesoporous ZnO Nanowires. *ACS Sensors* **2017**, *2*, 1567–1572, doi:10.1021/acssensors.7b00477.
  25. Tharsika, T.; Haseeb, A. S. M. A.; Akbar, S. A.; Mohd Sabri, M. F.; Hoong, W. Y. Enhanced ethanol gas sensing properties of SnO<sub>2</sub>-core/ZnO-shell nanostructures. *Sensors (Switzerland)* **2014**, *14*, 14586–14600, doi:10.3390/s140814586.
  26. Jeong, S.; Choe, M.; Kang, J. W.; Kim, M. W.; Jung, W. G.; Leem, Y. C.; Chun, J.; Kim, B. J.; Park, S. J. High-performance photoconductivity and electrical transport of ZnO/ZnS core/shell nanowires for multifunctional nanodevice applications. In *ACS Applied Materials and Interfaces*; 2014; Vol. 6, pp. 6170–6176.
  27. Li, T.; Zeng, W.; Wang, Z. Quasi-one-dimensional metal-oxide-based heterostructural gas-sensing materials: A review. *Sensors Actuators B Chem.* **2015**, *221*, 1570–1585, doi:10.1016/J.SNB.2015.08.003.
  28. Haque, M. J.; Bellah, M. M.; Hassan, M. R.; Rahman, S. Synthesis of ZnO nanoparticles by two different methods & comparison of their structural, antibacterial, photocatalytic and optical properties. *Nano Express* **2020**, *1*, 010007, doi:10.1088/2632-959x/ab7a43.
  29. Stafiniak, A.; Boratyński, B.; Baranowska-Korczyńska, A.; Szyszka, A.; Ramiączek-Krasowska, M.; Prazmowska, J.; Fronc, K.; Elbaum, D.; Paszkiewicz, R.; Tłaczała, M. A novel electrospun ZnO nanofibers biosensor fabrication. *Sensors Actuators B Chem.* **2011**, *160*, 1413–1418,

- doi:10.1016/J.SNB.2011.09.087.
30. Hosseini, Z. S.; zad, A. I.; Mortezaali, A. Room temperature H<sub>2</sub>S gas sensor based on rather aligned ZnO nanorods with flower-like structures. *Sensors Actuators B Chem.* **2015**, *207*, 865–871, doi:10.1016/J.SNB.2014.10.085.
  31. Fiedot, M.; Rac, O.; Suchorska-Woźniak, P.; Teterycz, H. Influence of a Morphology Sensitive Layer of Resistive Gas Sensors on Chlorine Sensing. *Procedia Eng.* **2016**, *168*, 1118–1121, doi:10.1016/J.PROENG.2016.11.363.
  32. Van Dang, T.; Duc Hoa, N.; Van Duy, N.; Van Hieu, N. Chlorine Gas Sensing Performance of On-Chip Grown ZnO, WO<sub>3</sub>, and SnO<sub>2</sub> Nanowire Sensors. *ACS Appl. Mater. Interfaces* **2016**, *8*, 4828–4837, doi:10.1021/acsami.5b08638.
  33. Patil, D. R.; Patil, L. A. Room temperature chlorine gas sensing using surface modified ZnO thick film resistors. *Sensors Actuators, B Chem.* **2007**, *123*, 546–553, doi:10.1016/j.snb.2006.09.060.
  34. Fiedot, M.; Karbownik, I.; Maliszewska, I.; Rac, O.; Suchorska-Woźniak, P.; Teterycz, H. Deposition of one-dimensional zinc oxide structures on polypropylene fabrics and their antibacterial properties. *Text. Res. J.* **2015**, *85*, 1340–1354, doi:10.1177/0040517514563716.
  35. Williamson, G. K.; Hall, W. H. X-ray line broadening from fided aluminium and wolfram. *Acta Metall.* **1953**, *1*, 22–31, doi:10.1016/0001-6160(53)90006-6.
  36. Zhang, X.; Qin, J.; Xue, Y.; Yu, P.; Zhang, B.; Wang, L.; Liu, R. Effect of aspect ratio and surface defects on the photocatalytic activity of ZnO nanorods. *Sci. Rep.* **2014**, *4*, doi:10.1038/srep04596.
  37. Kushwaha, A.; Aslam, M. Hydrogen-incorporated ZnO nanowire films: stable and high electrical conductivity. *J. Phys. D. Appl. Phys.* **2013**, *46*, 485104, doi:10.1088/0022-3727/46/48/485104.
  38. Ghobadi, A.; Ulusoy, T. G.; Garifullin, R.; Guler, M. O.; Okyay, A. K. A Heterojunction Design of Single Layer Hole Tunneling ZnO Passivation Wrapping around TiO<sub>2</sub> Nanowires for Superior Photocatalytic Performance. *Sci. Rep.* **2016**, *6*, doi:10.1038/srep30587.
  39. Thi Quy, C.; Xuan Thai, N.; Duc Hoa, N.; Thi Thanh Le, D.; Manh Hung, C.; Van Duy, N.; Van Hieu, N. C<sub>2</sub>H<sub>5</sub>OH and NO<sub>2</sub> sensing properties of ZnO nanostructures: correlation between crystal size, defect level and sensing performance., doi:10.1039/c7ra13702h.
  40. Saoud, K.; Alsoubaihi, R.; Bensalah, N.; Bora, T.; Bertino, M.; Dutta, J. Synthesis of supported silver nano-spheres on zinc oxide nanorods for visible light photocatalytic applications. *Mater. Res. Bull.* **2015**, *63*, 134–140, doi:10.1016/j.materresbull.2014.12.001.
  41. Gopel, W. REACTIONS OF OXYGEN WITH ZnO-1010-SURFACES. *J Vac Sci Technol* **1978**, *15*, 1298–1310, doi:10.1116/1.569757.
  42. Wang, D.; Hu, P.; Xu, J.; Dong, X.; Pan, Q. Fast response chlorine gas sensor based on mesoporous SnO<sub>2</sub>. *Sensors Actuators B Chem.* **2009**, *140*, 383–389, doi:10.1016/J.SNB.2009.05.027.
  43. Cotton, F. A.; Wilkinson, G.; Murillo, C. a.; Bochmann, M. *Advanced Inorganic Chemistry, 6th Edition*; 1999; ISBN 978-0-471-19957-1.
  44. Han, N.; Wu, X.; Chai, L.; Liu, H.; Chen, Y. Counterintuitive sensing mechanism of ZnO nanoparticle based gas sensors. *Sensors Actuators B Chem.* **2010**, *150*, 230–238, doi:10.1016/J.SNB.2010.07.009.
  45. Nundy, S.; Eom, T. yil; Kang, J. gu; Suh, J.; Cho, M.; Park, J. S.; Lee, H. J. Flower-shaped ZnO nanomaterials for low-temperature operations in NO<sub>x</sub> gas sensors. *Ceram. Int.* **2020**, *46*, 5706–5714, doi:10.1016/j.ceramint.2019.11.018.
  46. An, W.; Wu, X.; Zeng, X. C. Adsorption of O<sub>2</sub>, H<sub>2</sub>, CO, NH<sub>3</sub>, and NO<sub>2</sub> on ZnO nanotube: A density functional theory study. *J. Phys. Chem. C* **2008**, *112*, 5747–5755, doi:10.1021/jp711105d.